



Cite this: *Phys. Chem. Chem. Phys.*,  
2015, 17, 27588

# Mechanisms of fluorescence decays of colloidal CdSe–CdS/ZnS quantum dots unraveled by time-resolved fluorescence measurement

Hao Xu, Volodymyr Chmyrov, Jerker Widengren, Hjalmar Brismar and Ying Fu\*

By narrowing the detection bandpass and increasing the signal-to-noise ratio in measuring the time-resolved fluorescence decay spectrum of colloidal CdSe–CdS/ZnS quantum dots (QDs), we show that directly after the photoexcitation, the fluorescence decay spectrum is characterized by a single exponential decay, which represents the energy relaxation of the photogenerated exciton from its initial high-energy state to the ground exciton state. The fluorescence decay spectrum of long decay time is in the form of  $\beta/t^2$ , where  $\beta$  is the radiative recombination time of the ground-state exciton and  $t$  is the decay time. Our findings provide us with a direct and quantitative link between fluorescence decay measurement data and fundamental photophysics of QD exciton, thereby leading to a novel way of applying colloidal QDs to study microscopic, physical and chemical processes in many fields including biomedicine.

Received 29th May 2015,  
Accepted 16th September 2015

DOI: 10.1039/c5cp03109e

www.rsc.org/pccp

## 1 Introduction

Colloidal quantum dots (QDs) have been extensively studied,<sup>1–4</sup> developed<sup>5–8</sup> and utilized for many applications in many fields including biomedicine<sup>9–11</sup> and optoelectronics.<sup>12–15</sup> Extensive reviews about various aspects of QDs can be found readily in the literature.<sup>16–19</sup> Though the fundamental photophysics behind the superb and unique optical properties of these QDs is well understood, a quantitative match between theory and experiment is limited. One major issue is about the time-resolved fluorescence decay spectrum. A picosecond laser pulse is led into a QD ensemble,<sup>2,8,20–22</sup> or to a single QD,<sup>1</sup> and the QD fluorescence is detected as a function of time, denoted as  $F(t)$ , *i.e.*, the aforementioned time-resolved fluorescence decay spectrum. A multi-exponential model is commonly used to fit  $F(t)$ , and the number of exponential decay terms varies widely in the literature.<sup>5,8,14,21,23–27</sup> In ref. 27, Nadeau *et al.* used the one-state trapping model with three fitting parameters to fit the fluorescence decay spectra of mercaptopropionic acid (MPA) coated CdTe QDs under the influence of  $\beta$ -mercaptoethanol (BME), while the fitted data did not display clear relationships with the changes (pH value and BME concentration) in the QD solutions (note that the stretched model and two-exponential model were also used for comparison). It was reported recently<sup>4</sup> that  $F(t)$  was well described by the standard bi-exponential model

$$F(t) = F_0 + A_1 \exp\left(-\frac{t-t_0}{\tau_1}\right) + A_2 \exp\left(-\frac{t-t_0}{\tau_2}\right) \quad (1)$$

Science for Life Laboratory, Department of Applied Physics, Royal Institute of Technology, SE-106 91 Stockholm, Sweden. E-mail: fu@kth.se

both numerically (fitting convergence) and physically (the physical parameters in the above expression showed clear trends following the change in the QD environment). For 3-MPA coated CdSe–CdS/ZnS QDs dispersed in 4-(2-hydroxyethyl)-1-piperazine-ethanesulfonic acid (HEPES) buffer containing 50 mM HEPES and 23 mM NaOH with a pH value of 7.2,  $\tau_1 \approx 14$  ns while  $\tau_2 \approx 2$  ns, both of them decreased when  $\text{Ca}^{2+}$  ions were added to the QD solution and then recovered when  $\text{Ca}^{2+}$  ions were removed.<sup>4</sup>

Another fundamental issue is about the broad QD fluorescence peak. The full width at half maximum (FWHM) of the QD fluorescence peak is reported to be about 25 nm.<sup>28–30</sup> In aqueous solution this value is usually much larger. Such a broad peak is commonly attributed to the distribution of QD sizes in the QD solution.<sup>14,31</sup> A simple estimation using published formulae<sup>32</sup> showed that the large FWHM could be attributed to a distribution  $\delta r$  in QD radius  $r$  of  $\delta r/r \approx \pm 10\%$ , in agreement with high-resolution transmission electron microscopy (HRTEM) imaging.<sup>14</sup> On the other hand, the measured FWHM of single QDs was shown to be similar to the FWHM of a QD ensemble,<sup>33</sup> implying additional factor(s) in understanding the large FWHM of single QDs. Furthermore, a quantum Monte Carlo simulation of single QD fluorescence resulted in also a large FWHM when resonance and off-resonance radiative recombination processes of the ground-state exciton, *i.e.*, the broadening of the fluorescence peak from the time-dependent golden rule, were included in the simulation.<sup>32,34</sup>

In this work we study quantitatively the time-resolved fluorescence decay spectrum of water-soluble 3-MPA coated CdSe-based QDs as a function of the detection bandpass, detection wavelength, and integration time in order to unravel the principal



QD fluorescence decay processes and to explore the origins of the large FWHM of colloidal QDs.

## 2 Time-resolved fluorescence measurement

We focus on water-soluble CdSe–CdS/Cd<sub>0.5</sub>Zn<sub>0.5</sub>S/ZnS core-multishell QDs fabricated in-house using common recipes.<sup>4</sup> Standard structural characterization including core, shell, QD size distribution and surface ligands of these QDs have been performed, and details were published, see, *e.g.*, ref. 14 and 35. Consisting of a CdSe core, a CdS shell of 2 monolayers, another shell of 1 monolayer Cd<sub>0.5</sub>Zn<sub>0.5</sub>S, and 1.5 monolayer ZnS, these QDs were coated with 3-MPA surface ligands and had a fluorescence peak at 596 nm at room temperature. They were dispersed in HEPES buffer. These QDs were isolated single QDs confirmed experimentally by dropping 10  $\mu$ L QD solution on a microscope slide and then imaging using an AxioObserver.D1 microscope (Carl Zeiss) showing characteristic single QD blinking. All experimental measurements were performed at room temperature.

Electron energy levels in a QD is characterized by quantized exciton levels:<sup>36–38</sup> The valence-band sublevels in an as-grown QD are completely filled and the conduction-band sublevels are completely empty, which is denoted as the vacuum state  $\psi_0$ ; one electron initially occupying a valence-band sublevel transits to an empty conduction-band sublevel after absorbing a photon, leaving a hole in the valence-band sublevel. The electron and hole interact with each other *via* Coulombic interaction to form an exciton which is enforced by the spatial confinement of the nano-size QD. Since the excitation photon normally is high in energy, the photogenerated exciton is in an excited exciton state  $\psi_n$ . The excited exciton relaxes to the ground exciton state  $\psi_1$  *via* nonradiative interactions, and then radiatively recombines to emit a photon, *i.e.*, fluoresces, after which the QD returns to its vacuum state  $\psi_0$ .

The time-dependent wave function of the quantum state of the QD is

$$\sum_k C_k(t) \psi_k$$

where  $k$  runs over all exciton states. Writing the interaction potential  $s$  for either non-radiative energy relaxation or radiative photon emission as

$$V_s'^+ b_s e^{-i\omega_s t} + V_s' b_s^+ e^{i\omega_s t} \quad (2)$$

where  $b_s^+$  and  $b_s$  are the creation and annihilation operators, and  $\hbar\omega_s$  is the energy of the interaction such as a phonon (non-radiative energy relaxation) or a photon. Denoting the number of phonons or photons as  $N_s$ , the following equations for quantum state coefficients are obtained from the time-dependent Schrödinger equation

$$i\hbar \frac{dC_q(t)}{dt} = \sum_k C_k(t) \left[ \langle q|V_s'^+|k\rangle e^{i(E_q-E_k-\hbar\omega_s)t/\hbar} \sqrt{N_s} + \langle q|V_s'|k\rangle e^{i(E_q-E_k+\hbar\omega_s)t/\hbar} \sqrt{N_s+1} \right] \quad (3)$$

where  $E_k$  is the energy of state  $\psi_k$ . The first term on the right side of the equation describes the electron transition from state

$k$  to  $q$  accompanied by absorbing a phonon or a photon, *i.e.*,  $E_k + \hbar\omega_s \rightarrow E_q$ , while the second term is about emitting a phonon or a photon,  $E_k - \hbar\omega_s \rightarrow E_q$ .

The probability that the QD emits a photon at time  $t$  is proportional to

$$|\langle \psi_0|V_{\text{photon}}|\psi_1\rangle|^2 |C_1(t)|^2 [1 - |C_0(t)|^2] \quad (4)$$

For the radiative recombination,  $s$  represents the photon field, while the photoexcited exciton  $\psi_n$  normally undergoes many nonradiative energy relaxation processes through many other excited exciton states such as electron–phonon interactions in the QD semiconductor material and many transitions to and from surface states on the large superficial surface area of the colloidal QD before it reaches  $\psi_1$ . Therefore, the solution of eqn (3) requires the knowledge of the interaction potentials. More critically, it also needs to involve a large number of excited exciton states in order to obtain a full quantum mechanical description.

In order to quantitatively correlate the principal decay processes to the time-resolved fluorescence decay spectrum, we study the transition rates of the energy relaxation and radiative recombination of an exciton by the following principal decay processes:

- (1) Three principal exciton levels: excited exciton state  $\psi_n$  (energy  $E_n$ ), with its occupation  $n_n = |C_n|^2$ ; ground exciton state  $\psi_1$  ( $E_1$ ) with occupation  $n_1 = |C_1|^2$ ; vacuum state  $\psi_0$  ( $E_0$ ) with occupation  $n_0 = |C_0|^2$ .
- (2) Optical excitation to generate an exciton from vacuum to  $\psi_n$ .
- (3)  $\psi_n$ -exciton relaxes at a rate  $1/\tau$  to  $\psi_1$  nonradiatively.
- (4) Ground-state exciton transits radiatively to  $\psi_0$  at a rate  $1/\beta$ .

In the electron–hole picture, the photoexcitation of the QD is such that an electron originally occupying a valence band sublevel in the QD absorbs a photon to transit to an initially empty sublevel in the conduction band, leaving the valence band sublevel empty (a hole). The electron in the conduction band sublevel and the hole in the valence band sublevel interact with each other *via* Coulomb interaction to form an electron–hole pair (*i.e.*, exciton). The electron will relax to the ground sublevel in the conduction band, while the hole will relax to the ground sublevel in the valence band, forming the exciton ground state. The electron at the conduction-band ground sublevel transits to the empty valence-band ground sublevel (*i.e.*, the hole at the valence-band ground sublevel) to emit a photon (QD fluorescence), for which the conduction

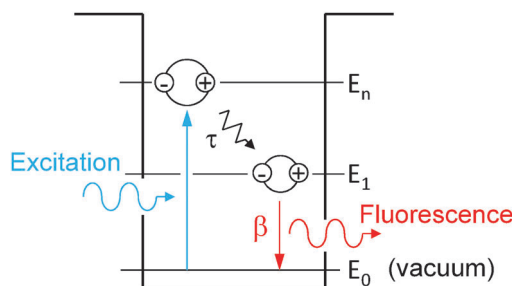


Fig. 1 Schematics of photogeneration, energy relaxation  $\tau$  and radiative recombination  $\beta$  of an exciton in the QD.



band sublevels are all empty and the valence band sublevels are all occupied. In other words, the QD returns to its vacuum state.

Following the fluorescence decay experimental procedure, the QD is initially at its vacuum state. One pulsed excitation excites the QD at  $t = 0$  so that  $n_n = 1$  and  $n_1 = n_0 = 0$ . The decay processes, schematically shown in Fig. 1, are described mathematically by the following rate equations:

$$\begin{aligned}\frac{dn_n}{dt} &= -\frac{n_n(1-n_1)}{\tau} \\ \frac{dn_1}{dt} &= \frac{n_n(1-n_1)}{\tau} - \frac{n_1(1-n_0)}{\beta} \\ \frac{dn_0}{dt} &= \frac{n_1(1-n_0)}{\beta}\end{aligned}\quad (5)$$

which have been commonly applied to study multi-level multi-electron systems, see, e.g., ref. 39 and 40. The key factor here is the Pauli exclusion principle (Fermion anticommutation relationships of the electron creation and annihilation operators) that the occupation of one exciton level reduces the efficiencies of transitions to this exciton level since each exciton level can be occupied by only one exciton. As a consequence, the transition efficiency of an exciton from an initial exciton level to a final exciton level is determined by both the occupation of the initial level and the un-occupation of the final level.<sup>40</sup>

We performed a numerical simulation of eqn (5) using  $\tau = 8.0$  ns and  $\beta = 2.0$  ns (see more discussions about values of  $\tau$  and  $\beta$  below). Temporal developments of  $n_n$ ,  $n_1$ ,  $n_0$ , and the theoretical time-resolved fluorescence decay spectrum,

$$f(t)|_{t=\ell\delta} = \int_{(\ell-1)\delta}^{\ell\delta} \frac{n_1(1-n_0)}{\beta} dt \quad (6)$$

are presented in Fig. 2(a) in a logarithmic scale. Here we tried to simulate the measurement procedure that  $\delta$  is the integration time of time-to-amplitude-converter (TAC) channels (see below). We observe two distinct decay characters in  $f(t)$ , a rather fast decay directly after the optical excitation and a slow decay when  $t$  is long.

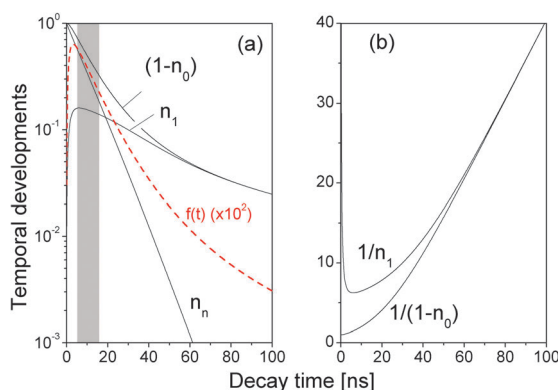


Fig. 2 (a) Temporal developments of  $n_n$ ,  $n_1$ ,  $(1-n_0)$ , and the theoretical time-resolved fluorescence decay spectrum  $f(t)$  (red line, magnified by  $10^2$ ).  $\tau = 8.0$  ns,  $\beta = 2.0$  ns. (b)  $1/n_1$  and  $1/(1-n_0)$ .  $\delta = 0.1$  ns.

In a very short time directly after the optical excitation, see the shadow area in Fig. 2(a),  $f_1(t)$  was well characterized by a single decay term

$$f_1(t) \propto e^{-t/\tau'} \quad (7)$$

for  $t \in (5, 15)$  ns. Subscript “1” in  $f_1(t)$  indicates the fluorescence decay spectrum of short  $t$ . Note that  $\tau'$  depends on both  $\tau$  and  $\beta$ , especially when the orders of  $\tau$  and  $\beta$  are close to each other. In the case of  $f(t)$  presented in Fig. 2(a) ( $\tau = 8.0$  and  $\beta = 2.0$  ns),  $\tau' = 11.10$  ns.

A close examination shows that the time-resolved fluorescence character for  $t > 60$  ns is very different from the exponential decay of  $f_1(t)$ . For  $t > 60$  ns, Fig. 2(a) shows that  $n_n$  is negligibly small so eqn (5) reduced to

$$\frac{dn_1}{dt} = -\frac{n_1(1-n_0)}{\beta}, \quad \frac{dn_0}{dt} = \frac{n_1(1-n_0)}{\beta} \quad (8)$$

Let  $1-n_0 = n_0'$  and  $n_1 = n_0'$ , the solution of the above equations is

$$\frac{1}{n_1} = \frac{1}{n_0'} = \frac{t+a}{\beta} \quad (9)$$

where  $a$  is a constant. The above solution is confirmed by the numerical results of  $1/n_1$  and  $1/(1-n_0)$  presented in Fig. 2(b). The long-time fluorescence decay for  $t > 60$  ns is thus

$$f_2(t)|_{t=\ell\delta} = \int_{(\ell-1)\delta}^{\ell\delta} \frac{n_1(1-n_0)}{\beta} dt \approx \frac{\beta\delta}{(t+a)^2} \Big|_{t=\ell\delta} \quad (10)$$

since the variations of  $n_1$  and  $(1-n_0)$  in  $t$  is very small in the time duration  $\in ((\ell-1)\delta, \ell\delta)$ . The above expression is hardly exponential and needs many exponential decay terms in order to fit it numerically.

By re-examining all our previously reported time-resolved fluorescence decay spectra  $F(\ell)$  such as in ref. 4 and 41, we indeed found out that the long-time fluorescence decay spectra matched perfectly with  $f_2(t)$  in eqn (10) by plotting  $\sqrt{1/F(\ell)}$  vs.  $\ell$  which was linear in  $\ell$  in a certain range of  $\ell$ , where  $F(\ell)$  is the measured time-resolved fluorescence decay spectrum as a function of TAC channel index  $\ell$ . A typical result is shown in Fig. 3. However, the results were not totally unambiguous due to the low signal-to-noise ratios when  $\ell$  was large.

We performed new time-resolved fluorescence measurements of our QDs in the following manner by using a time-correlated single-photon counting machine (FluoroMax-3, Horiba Jobin Yvon). A spectral line centered at 495 nm with a 2 nm bandpass from a pulsed light-emitting diode (peak wavelength 495 nm and 30 nm FWHM) was led to the cuvette containing the QD aqueous solution in the form of a train of pulses (pulse duration was ca. 1.4 ns) at 1 MHz. The detector was set at 596 nm (QD fluorescence peak wavelength) with a bandpass of 2 nm. There were 2048 TAC channels with a variable integration time  $\delta$  so that the measurement decay time ranged from 50 ns to 1  $\mu$ s. The photon counting was stopped when the maximal number of photon counts of the TAC channels reached a pre-set maximal photon-count value  $N_{\max}$ .  $\delta$  and  $N_{\max}$  were adjusted in order to reach a high signal-to-noise ratio.



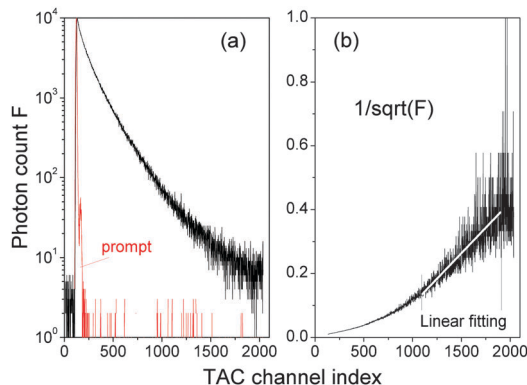


Fig. 3 (a) Time-resolved fluorescence decay spectrum  $F(\ell)$  as a function of the time-to-amplitude-converter channel (TAC) index  $\ell$ . (b)  $\sqrt{1/F(\ell)}$  and a linear fitting in the TAC channel range of  $\ell \in (1100, 1900)$ .  $\delta = 0.1148971$  ns and  $t = \ell\delta$  is the decay time.

In order to compare the experimental decay spectrum with eqn (7) and (10), we normalized  $F(\ell)$

$$f_n(\ell) = \frac{F(\ell)}{N_{\max}} \quad (11)$$

$1/\sqrt{f_n(\ell)}$  of various  $N_{\max}$  and  $\delta$  are presented in Fig. 4. The dashed horizontal line in Fig. 4(a) showed that the noise levels before and long after the excitation pulse were aligned, ensuring that the QD fluorescence was excited by a single light pulse. The signal-to-noise ratio was significantly improved when  $N_{\max}$  was increased.

In order to efficiently utilize the TAC channels, we decreased  $\delta$  and the results are presented in Fig. 4(b) and (c). While Fig. 4(c) is commonly reported in literature, its time range is too short to

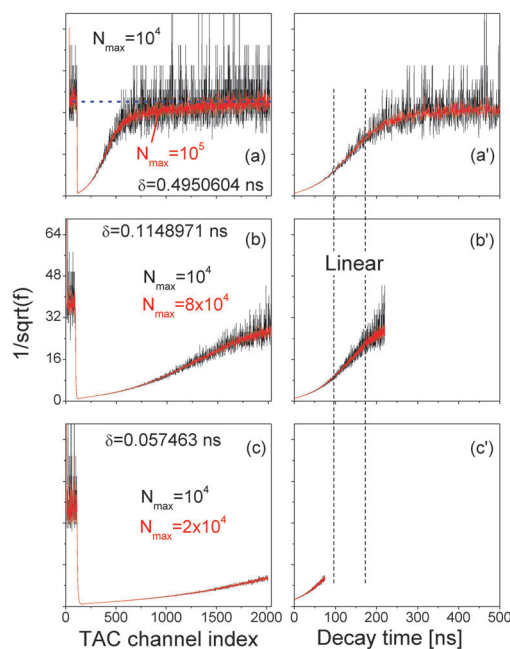


Fig. 4 (a, b and c)  $\sqrt{1/f_n(\ell)}$  vs. TAC channel index  $\ell$  as a function of  $N_{\max}$  and  $\delta$ . (a', b' and c')  $1/\sqrt{f_n(\ell\delta)}$  vs. decay time  $t = \ell\delta$ .

unravel the linear range between the two vertical dashed lines in Fig. 4(a')–(c') that is directly correlated with the exciton radiative recombination process.

In Fig. 3 and 4, the data were recorded from a QD ensemble in aqueous solution, whereas the model of Fig. 2 applies for one exciton in a single QD. The assumption of one exciton per one QD is valid in our experimental setup since the excitation laser is too weak to excite multiple excitons. The issue of a single QD vs. an ensemble of single QDs needs a close examination (the QDs in solution were isolated single QDs because they were blinking under continuous excitation). The peak of the fluorescence of a QD solution is normally quite broad with a FWHM typically about 25 nm. It is generally accepted, as mentioned before, that the broad fluorescence peak of QDs in solution is due to the distribution of QD sizes. What we did in measuring the time-resolved fluorescence decay spectra here was to reduce the bandpass of the detector to only 2 nm so that we collected only the fluorescence signals from QDs of one size, if QD size distribution is the sole cause of the broad FWHM. Our experimentally measured time-resolved fluorescence decay spectra thus complied with the pre-assumptions of eqn (7) and (10) and therefore can be described by eqn (7) and (10).

Fig. 4 shows a clear match between the long-time time-resolved fluorescence and eqn (10). It is thus concluded that the time-resolved fluorescence decay spectrum reflects directly and quantitatively the energy relaxation and the radiative recombination of the exciton in the QD.

### 3 Fluorescence spectrum of single QDs

As mentioned before, we studied the QD fluorescence spectrum by applying the time-dependent quantum Monte Carlo simulation method that included radiative and non-radiative resonance and off-resonance transitions among confined exciton states and found that the fluorescence peak of a single QD was intrinsically broad due to resonance and off-resonance exciton radiative recombinations from the time-dependent golden rule.<sup>32,34</sup> To validate this theoretical result, we tried to measure the fluorescence spectra of single QDs. A drop of the QD solution was deposited into a circular area formed by nail polish on a microscope slide then covered by a coverslip. Fluorescence emissions from QDs deposited on the microscope slide were excited by a 488 nm excitation laser using a confocal microscope (Zeiss LSM 780) with a  $63\times/1.4$  oil immersion objective (Carl Zeiss) and recorded over a bandwidth of 562–637 nm with a spectral resolution of 2.9 nm. The image frame size was  $26.99 \times 26.99 \mu\text{m}^2$  ( $512 \times 512$  pixels). Software ImageJ was used to obtain the fluorescence spectra of single QDs.

Two QD samples were prepared and studied. One was quite diluted (QD concentration 10 pM) so that the optical spectra of single QDs were obtained, see Fig. 5(a). The other sample contained highly concentrated QDs which resulted in an optical spectrum of a QD ensemble, see Fig. 5(b).

The fluorescence spectra of 15 randomly chosen single QDs from the diluted sample (a) are presented in Fig. 5(c) as black



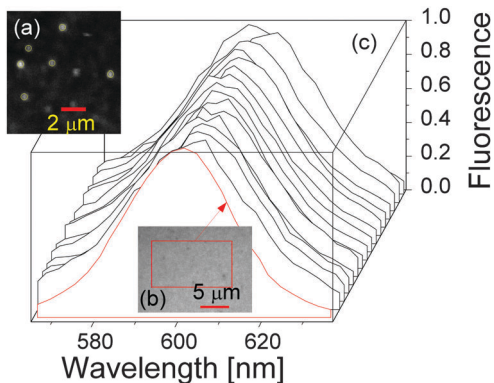


Fig. 5 (a) One image frame showing the spatial locations of single QDs in the diluted sample. (b) One image frame of the highly concentrated QDs. (c) Fluorescence spectra of single QDs (black lines) and the compact QD ensemble (red line).

solid lines, together with the optical spectrum of the QD ensemble from sample (b), indicating that the optical spectra of single QDs and the QD ensemble are very similar. Note that the fluorescence spectrum of the QD ensemble in sample (b) was identical to the one of QDs in solution in the cuvette for the time-resolved fluorescence decay measurements. Straightforward spectral analysis showed that the FWHMs of the QD ensemble and QDs in solution were *ca.* 33 nm, and the averaged FWHM of the 15 single QDs was also around 33 nm with individual FWHMs ranging from 32 nm to 39 nm.

We examined the spectral diffusion of our confocal microscope by measuring the spectrum of the excitation laser light reflected from the microscopic slide. The FWHM of the reflected spectral peak was less than 5 nm (see also ref. 42), far narrower than the QD fluorescence peak. It was therefore safe to conclude that the large FWHM (*ca.* 33 nm) of the single QD fluorescence peak is intrinsic.

## 4 Resonance and off-resonance fluorescence lifetimes

From the scattering theory and the generalized Fermi golden rule, the temporal development  $\hat{T}$  of exciton state  $\psi_1$  is described by<sup>41,43</sup>

$$\langle \psi_1 | \hat{T}(t) | \psi_1 \rangle \approx e^{-w_1 t/2} \quad (12)$$

where  $1/w_1$  is the decay time of  $\psi_1$ , which is given as

$$w_1(\hbar\omega) = \frac{2\pi}{\hbar} \left| \left\langle \psi_0 \left| \sum_i V_i \right| \psi_1 \right\rangle \right|^2 \frac{\Gamma_1}{\Gamma_1^2 + (E_1 - E_0 - \hbar\omega)^2} \quad (13)$$

$E_1$  and  $E_0$  are energies of  $\psi_1$  and  $\psi_0$ , respectively.  $\hbar\omega$  is the photon energy.  $V_i$  is the  $i$ th interaction between  $\psi_1$  and  $\psi_0$ .  $\Gamma_1 = \hbar w_1/2$  is the relaxation energy of  $\psi_1$  due to interactions  $V_i$  with  $\psi_0$ .

Eqn (13) implies a short resonance fluorescence lifetime (*i.e.*, large  $w_1$  when  $E_1 - E_0 - \hbar\omega = 0$ ) and a long off-resonance fluorescence lifetime. We therefore tried to find the origin of the large FWHM of our QDs by tuning the detection wavelength of our time-resolved fluorescence decay measurement setup to

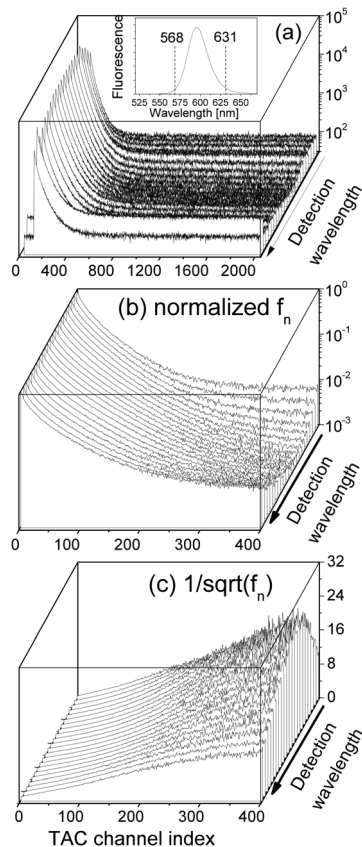


Fig. 6 (a) Time-resolved fluorescence decay spectra  $F(\ell)$  of our QD solution measured at different detection wavelengths  $\in$  (568, 631) nm while the detection bandpass was fixed to be 1 nm. The inset shows the fluorescence spectrum of the QD solution. (b) Normalized  $f_n(\ell)$ . (c)  $1/\sqrt{f_n(\ell)}$ .  $\delta = 0.4950604$  ns.

scan our QD fluorescence peak with a bandpass of only 1 nm which was much smaller than the FWHM of our QDs. The measured fluorescence decay spectra  $F(\ell)$  at various detection wavelengths are presented in Fig. 6(a). Here  $\delta = 0.4950604$  ns while  $N_{\max}$  were preset to  $10^5$ . At off-resonance wavelengths we had to reduce  $N_{\max}$  in order to obtain  $F(\ell)$  within a reasonable time before the laser pulse train heated up the QDs.

We normalized  $F(\ell)$  to obtain  $f_n(\ell)$  by eqn (11), which are presented in Fig. 6(b) showing a strong detection-wavelength dependence of the fluorescence decay, especially at long decay time, which is much better visualized in  $1/\sqrt{f_n(\ell)}$  in Fig. 6(c). More profoundly, the profile of the long-time  $1/\sqrt{f_n(\ell)}$  vs. the detection wavelength is almost identical to the fluorescence spectrum of our QDs shown as the inset in Fig. 6(a).

Note that the measured spectrum  $f_n(\ell)$  of eqn (11) is a convolution of the time-resolved fluorescence  $f(t)$  defined by eqn (6) and the instrumental response function  $p(\ell)$  of the time-correlated single-photon counting machine, *i.e.*, the prompt signal shown in Fig. 3(a). We used software DAS6 v6.1 (decay analysis software with de-convolution) that takes the instrumental response function into account to fit  $F(\ell)$  in Fig. 6(a) in a photon count range of  $\in$  (0.9, 0.5) $N_{\max}$  by a single decay term  $e^{-t/\tau}$ . Since  $p(\ell)$  of our system is very narrow in  $\ell$



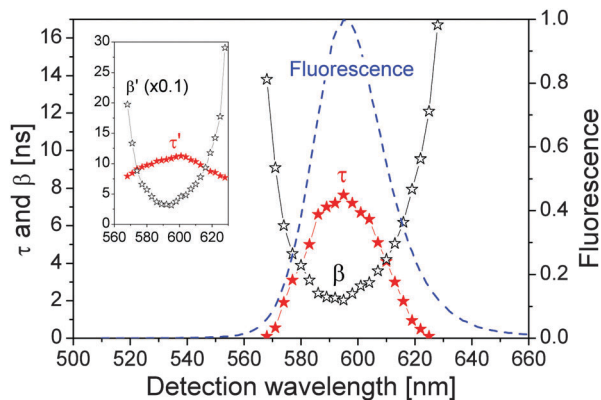


Fig. 7 Fitting parameters as a function of detection wavelength. Solid stars:  $\tau$ ; hollow stars:  $\beta$ . The normalized QD fluorescence spectrum is presented as a dashed line for comparison. The inset shows  $\tau'$  and  $\beta'$  ( $\beta'$  is scaled down by a factor of 10).

while the variation of  $f_2(t)$  (long decay time  $t$ ) in  $t$  is rather small, the effects of the numerical de-convolution of  $p(\ell)$  and  $F(\ell)$  at large  $\ell$  are negligible so that we could fit directly the spectra in Fig. 6(c) by eqn (10) to obtain  $\beta'$ . The resulting  $\tau'$  and  $\beta'$  are presented in the inset of Fig. 7 (the value of  $\beta'$  was scaled down by a factor of 10).

Moreover, the  $(0.9, 0.5)N_{\max}$  range in obtaining  $\tau'$  *i.e.*, the grey region in Fig. 2(a), is determined by the time window after  $n_1$  reaches its peak value and before  $n_n$  decreases below  $n_1$ , within which the fluorescence decay spectrum can be well approximated by a single exponential decay.

We adjusted  $\tau$  and  $\beta$  in eqn (5) so that  $f(t)$  from eqn (6) had the same  $\tau'$  and  $\beta'$  in the inset of Fig. 7, which are presented in Fig. 7 showing that both  $\tau$  and  $\beta$  depend strongly on the detection wavelength. Most importantly, the relationships between  $\tau$  and  $1/\beta$  and the detection wavelength agree well with the QD fluorescence spectrum. At the QD fluorescence peak wavelength,  $\tau = 8.0$  ns and  $\beta = 2.0$  ns which were used in calculating Fig. 2.

The strong dependences of  $\tau$  and  $\beta$  on the detection wavelength and their symmetry with respect to the fluorescence peak wavelength suggest that the large FWHM of our QDs is most probably due to the resonance and off-resonance exciton radiative recombination processes, instead of being dominantly determined by the QDs' size distribution (since it is expected physically that the changes in  $\tau$  and  $\beta$  as functions of the QD size should be monotonic).

As shown in Fig. 1,  $\tau$  describes the energy relaxation from the excited exciton state  $\psi_n$  to the ground exciton state  $\psi_1$ . The energy relaxation processes in common semiconductors are electron–phonon interactions. The energy of the most active optical phonons is  $\hbar\omega_p = 37$  meV in bulk CdSe.<sup>44,45</sup> Similar to eqn (13), the rate of the electron–phonon (“ep”) interaction between two exciton states  $\psi_n$  and  $\psi_1$  is proportional to

$$w_{\text{ep}} = \frac{2\pi}{\hbar} |\langle \psi_1 | V_{\text{ep}} | \psi_n \rangle|^2 \frac{\Gamma_p}{\Gamma_p^2 + (E_n - E_1 - \hbar\omega_p)^2} \quad (14)$$

where  $\Gamma_p$  is the relaxation energy of the electron–phonon interaction.  $w_{\text{ep}}$  is maximal when  $E_n - E_1 = \hbar\omega_p$ . Because  $\hbar\omega_p$  of semiconductor nanostructures remained the same as in the bulk material,<sup>41</sup> while the exciton states in quantum nanostructures are discrete, the electron–phonon interaction rate in a semiconductor nanostructure can be very low when  $E_n - E_1 \neq \hbar\omega_p$ , which is known as the phonon bottleneck, see, *e.g.*, ref. 36 and 46. Note that the electron–phonon interactions between high-energy exciton states in our QDs are not expected to be much limited due to the high density of exciton states as well as small energy separations between them.<sup>47</sup> We thus can expect a peak of  $\tau = 1/w_{\text{ep}}$  centered at  $E_1$ , as shown in Fig. 7. Moreover, the FWHM of the  $\tau$  distribution peak of our QDs is about 33 nm (*ca.* 110 meV, the same as the FWHM of the QD fluorescence peak), which is larger than  $2\hbar\omega_p = 74$  meV which is expected when the electron–phonon interaction is the dominant factor in determining  $\tau$ . One very possible reason for the relatively large FWHM is that we approximated many high-energy exciton states by a single state  $E_n$  in eqn (14).

$\beta$  describes the radiative recombination of the ground exciton state  $\psi_1$  to vacuum state  $\psi_0$ . By including only the light–matter interaction between  $\psi_1$  and  $\psi_0$ , *i.e.*, the radiative recombination process in eqn (13), it was estimated that for our QDs of radius 5 nm and  $E_1 - E_0 = 595$  nm,  $\Gamma_1 = 0.25$  meV and  $1/w_1 = \beta = 1.3$  ps at resonance ( $E_1 - E_0 - \hbar\omega = 0$ ).<sup>41</sup> It is then easy to estimate by eqn (13) that at off-resonance of  $\hbar\omega = 595 \pm 1$  nm,  $\beta_{\pm 1} = 0.25$  ns. And at off-resonance of  $\hbar\omega = 595 \pm 10$  nm,  $\beta_{\pm 10} = 26$  ns. These numbers agreed well with  $\beta$  in Fig. 7. Note that  $\beta = 1.3$  ps was estimated for the radiative recombination at resonance for our QDs. At off-resonance of  $\pm 10$  nm,  $\beta_{\pm 10} = 26$  ns, which is four orders of magnitude longer than in the resonance situation, due to the small  $\Gamma_1 = 0.25$  meV, while the energy difference between photons at wavelength 595 nm and 585 nm is 35.6 meV. In realistic measurements, the detection bandwidth is always finite so that it is very difficult to realize the perfect resonance condition. Moreover, there are nonradiative recombination processes as well as electron–phonon-interaction-assisted optical transition.<sup>48</sup> These two factors are most possibly the major reasons that reported radiative recombination time in CdSe QDs is in the order of nanoseconds, *e.g.*, see ref. 49 and 50.

## 5 Discussion

At the fluorescence peak wavelength, the extracted energy relaxation time of  $\tau = 8$  ns with a detection bandpass of 2 nm, see Fig. 7, is much longer than many individual energy relaxation processes in nanometer CdSe and CdSe/ZnS heterostructures, such as the ps-order Auger-type energy relaxation process,<sup>47,51</sup> and ps-order 1P-to-1S intraband electron relaxation obtained by measuring femtosecond transient absorption of CdSe QDs.<sup>52</sup> On the other hand, there have been extensive experimental studies demonstrating long relaxation times in the order of ns in nanostructures, *e.g.*, see ref. 53 and 54. Relaxation time longer than 1 ns was reported in colloidal CdSe QDs.<sup>55</sup> A major difference between the short and long energy relaxation processes is that



the former involves limited numbers of discrete energy levels and energy relaxation processes, while the numbers of energy levels and energy relaxation processes in the latter are much higher. When multiple phonon effects were included in a perturbation calculation, a ns-order electron energy relaxation was obtained.<sup>56</sup> We further notice the fact that the density of exciton states in the QD increases drastically when the exciton energy becomes higher than the energy of the ground exciton state, see, *e.g.*, ref. 47, which is clearly reflected in the absorption spectrum of the QD that the absorption of the QD increases very quickly when the photon energy exceeds the energy of the first absorption peak. Another critical aspect about colloidal QDs is their huge superficial surfaces and a large number of surface ligands which can trap either the electron or the hole to prolong the energy relaxation processes. In other words, the representative exciton state  $\hbar\omega_n$  in Fig. 1 represents a group of exciton states undergoing many energy relaxation processes and there are many exciton states between  $\psi_n$  and  $\psi_1$ .

We applied eqn (7) and (10) to fit our previously reported time-resolved fluorescence decay spectra<sup>4</sup> of QDs in the presence of free  $\text{Ca}^{2+}$  ions and EGTA (ethylene glycol tetraacetic acid, which chelates  $\text{Ca}^{2+}$ ), which were analyzed by the bi-exponential model of eqn (1). The QDs here had a fluorescence peak wavelength of 607 nm.  $N_{\text{max}}$  was 10 000, the excitation laser wavelength was 495 nm, the center of the detector wavelength was 607 nm, and the detection bandpass was 2 nm. The extracted  $\tau$  decreased while  $\beta$  increased following monotonically the increase of the  $\text{Ca}^{2+}$  concentration. They recovered when EGTA was added which chelated  $\text{Ca}^{2+}$  in the QD solution. This confirms the proposed mechanisms that the introduction of  $\text{Ca}^{2+}$  at the QD surface attracts the photogenerated electron and repels the hole, facilitating the transport of the electron and the hole between exciton states in the QD core and surface states by applying the surface-state associated blinking model, see *e.g.* ref. 57. The energy relaxation time  $\tau$  was reduced because of the increased energy relaxation channels, *i.e.*, the number of  $V_i$  terms in eqn (13), at the QD surface (including surface states). Furthermore, because of the increased spatial separation between the electron and the hole,  $\left\langle \psi_0 \left| \sum_i V_i \right| \psi_1 \right\rangle$  in eqn (13) is reduced, resulting in a reduced radiative recombination of the exciton and thereafter an increased  $\beta$ .

The effect of surface states to the fluorescence decay discussed in the above paragraph agreed with the further observation reported in ref. 4 that at the same time  $\tau$  was decreased following the  $\text{Ca}^{2+}$  concentration increase in the QD solution, the on-state probability in the single QD blinking was reduced since a  $\text{Ca}^{2+}$  ion at the QD surface increased the effect of surface states. In ref. 1, Fisher *et al.* reported that in the emission-intensity trajectory, the fluorescence decay was long when the fluorescence intensity was high, and single-exponential fluorescence decay was observed at maximum fluorescence intensities. The experimental data can be well understood by the correlation between surface states and  $\tau$ . At maximum fluorescence intensities, the effect of surface states to  $\tau$  is minimal so that the energy relaxation process of an exciton from  $\psi_n$  to  $\psi_1$  will be

slow, *i.e.*,  $\tau$  is long compared with  $\beta$ . In this case, the fluorescence decay is dominantly determined by the single-exponential decay from  $\psi_n$  to  $\psi_1$  since an exciton occupying  $\psi_1$  will transit quickly to  $\psi_0$  (short  $\beta$ ) as compared with the exciton relaxation from  $\psi_n$  to  $\psi_1$  (long  $\tau$ ). In different situations when  $\tau$  is comparable with  $\beta$  we expect different decay characters in different time windows.

## 6 Summary

By narrowing the detection bandpass and increasing the signal-to-noise ratio in measuring the time-resolved fluorescence decay spectrum of colloidal CdSe–CdS/ZnS QDs, we have shown that directly after the photoexcitation, QD's fluorescence decay spectrum is characterized by an exponential decay due to the energy relaxation of the photogenerated exciton from its initial high-energy exciton state to the largely empty ground exciton state. At long decay time, the high-energy exciton state is basically empty, and the fluorescence is determined by the radiative recombination of the exciton from the ground exciton state to the vacuum state, both states are now partially occupied. Because of the Pauli exclusion principle, the long-time fluorescence decay spectrum is in the form of  $\beta/t^2$ , which is hardly exponential. Here  $\beta$  is the radiative recombination time of the ground-state exciton and  $t$  is the decay time. Furthermore,  $\beta$  is minimal at the fluorescence peak wavelength suggesting that the observed broad QD fluorescence peak is most probably due to resonance and off-resonance exciton radiative recombination processes.

Colloidal quantum dots (QDs) have been the subject of extensive research and technical development. Time-resolved fluorescence decay spectroscopy has been widely used as an effective method to characterize QDs in various environments. Our work unravels quantitatively the link between the fluorescence decay of QDs and microscopic physical and chemical processes in the environment surrounding the QDs. We believe that our work will be very useful, providing new analyses of time-resolved fluorescence spectra of QDs opening up new means for the optical detection and studies of microscopic, physical and chemical events.

## Acknowledgements

This work was supported by Swedish Research Council (621-2011-4381) and the Knut and Alice Wallenberg Foundation (KAW 2011.0218).

## References

- 1 B. R. Fisher, H. J. Eisler, N. E. Stott and M. G. Bawendi, *J. Phys. Chem. B*, 2004, **108**, 143–148.
- 2 B. Mahler, P. Spinicelli, S. Buil, X. Quelin, J. P. Hermier and B. Dubertret, *Nat. Mater.*, 2008, **7**, 659–664.
- 3 O. Chen, J. Zhao, V. P. Chauhan, J. Cui, C. Wong, D. K. Harris, H. Wei, H. S. Han, D. Fukumura, R. K. Jain and M. G. Bawendi, *Nat. Mater.*, 2013, **12**, 445–451.



- 4 L. Li, Y. Chen, G. Tian, V. Akpe, H. Xu, L. M. Gan, S. Skrtic, Y. Luo, H. Brismar and Y. Fu, *J. Phys. Chem. C*, 2014, **118**, 10424–10433.
- 5 M. Jones, J. Nedeljkovic, R. J. Ellingson, A. J. Nozik and G. Rumbles, *J. Phys. Chem. B*, 2003, **107**, 11346–11352.
- 6 S. Hohng and T. Ha, *ChemPhysChem*, 2005, **6**, 956–960.
- 7 Y. Xing, Q. Chaudry, C. Shen, K. Y. Kong, H. E. Zhau, L. W. Chung, J. A. Petros, R. M. O'Regan, M. V. Yezhelyev, J. W. Simons, M. D. Wang and S. Nie, *Nat. Protoc.*, 2007, **2**, 1152–1165.
- 8 V. Fomenko and D. J. Nesbitt, *Nano Lett.*, 2008, **8**, 287–293.
- 9 M. Mahmoudi, V. Serpooshan and S. Laurent, *Nanoscale*, 2011, **3**, 3007–3026.
- 10 H. Mattoussi, G. Palui and H. B. Na, *Adv. Drug Delivery Rev.*, 2012, **64**, 138–166.
- 11 T. Ichimura, T. Jin, H. Fujita, H. Higuchi and T. M. Watanabe, *Front. Physiol.*, 2014, **5**, 273.
- 12 I. Tanaka, K. Kajimoto, K. Uno, O. Ohtsuki, T. Murase, H. Asami, M. Hara and I. Kamiya, *Jpn. J. Appl. Phys.*, 2005, **44**, L249–L252.
- 13 G. Konstantatos, I. Howard, A. Fischer, S. Hoogland, J. Clifford, E. Klem, L. Levina and E. H. Sargent, *Nature*, 2006, **442**, 180–183.
- 14 Z. Ning, H. Tian, H. Qin, Q. Zhang, H. Ågren, L. Sun and Y. Fu, *J. Phys. Chem. C*, 2010, **114**, 15184–15189.
- 15 T. You, L. Jiang, K. L. Han and W. Q. Deng, *Nanotechnology*, 2013, **24**, 245401(6).
- 16 I. L. Medintz, H. Mattoussi and A. R. Clapp, *Int. J. Nanomed.*, 2008, **3**, 151–167.
- 17 C. M. Evans, L. C. Cass, K. E. Knowles, D. B. Tice, R. P. H. Chang and E. A. Weiss, *J. Coord. Chem.*, 2012, **65**, 2391–2414.
- 18 J. Y. Kim, O. Voznyy, D. Zhitomirsky and E. H. Sargent, *Adv. Mater.*, 2013, **25**, 4986–5010.
- 19 X. Cheng, S. B. Lowe, P. J. Reece and J. J. Gooding, *Chem. Soc. Rev.*, 2014, **43**, 2680–2700.
- 20 S. F. Wuister, C. de Mello Donega and A. Meijerink, *J. Chem. Phys.*, 2004, **121**, 4310–4315.
- 21 D. Ratchford, K. Dziatkowski, T. Hartsfield, X. Li, Y. Gao and Z. Tang, *J. Appl. Phys.*, 2011, **109**, 103509(6).
- 22 U. O. S. Seker, E. Mutlugun, P. L. Hernandez-Martinez, V. K. Sharma, V. Lesnyak, N. Gaponik, A. Eychmüller and H. V. Demir, *Nanoscale*, 2013, **5**, 7034–7040.
- 23 D. Dorfs, T. Franzl, R. Osovsky, M. Brumer, E. Lifshitz, T. A. Klar and A. Eychmüller, *Small*, 2008, **4**, 1148–1152.
- 24 K. E. Knowles, E. A. McArthur and E. A. Weiss, *ACS Nano*, 2011, **5**, 2026–2035.
- 25 Y. C. Lin, W. C. Chou, A. S. Susha, S. V. Kershaw and A. L. Rogach, *Nanoscale*, 2013, **5**, 3400–3405.
- 26 E. Yaghini, F. Giuntini, I. M. Eggleston, K. Suhling, A. M. Seifalian and A. J. MacRobert, *Small*, 2013, **10**, 782–792.
- 27 J. L. Nadeau, L. Carlini, D. Suffern, O. Ivanova and S. E. Bradforth, *J. Phys. Chem. C*, 2012, **116**, 2728–2739.
- 28 J. J. Li, Y. A. Wang, W. Z. Guo, J. C. Keay, T. D. Mishima, M. B. Johnson and X. G. Peng, *J. Am. Chem. Soc.*, 2003, **125**, 12567–12575.
- 29 J. Muller, J. M. Lupton, A. L. Rogach, J. Feldmann, D. V. Talapin and H. Weller, *Phys. Rev. Lett.*, 2004, **93**, 167402.
- 30 D. E. Gomez, J. van Embden and P. Mulvaney, *Appl. Phys. Lett.*, 2006, **88**, 154106.
- 31 D. Pal, V. G. Stoleru, E. Towe and D. Firsov, *Jpn. J. Appl. Phys.*, 2002, **41**, 482–489.
- 32 Y. Fu, T. T. Han, H. Ågren, L. Lin, P. Chen, Y. Liu, G. Q. Tang, J. Wu, Y. Yue and D. Dai, *Appl. Phys. Lett.*, 2007, **90**, 173102(3).
- 33 L. Li, G. Tian, Y. Luo, H. Brismar and Y. Fu, *J. Phys. Chem. C*, 2013, **117**, 4844–4851.
- 34 T. T. Han, Y. Fu and H. Ågren, *J. Appl. Phys.*, 2007, **101**, 063712(6).
- 35 Z. J. Ning, M. Molnár, Y. Chen, P. Friberg, L. M. Gan, H. Ågren and Y. Fu, *Phys. Chem. Chem. Phys.*, 2011, **13**, 5848–5854.
- 36 R. Heitz, H. Born, F. Guffarth, O. Stier, A. Schliwa, A. Hoffmann and D. Bimberg, *Phys. Rev. B: Condens. Matter Mater. Phys.*, 2001, **64**, 241305(4).
- 37 Y. Fu, S. Hellström and H. Ågren, *J. Nonlinear Opt. Phys. Mater.*, 2009, **18**, 195–226.
- 38 Y. Fu, *J. Appl. Phys.*, 2009, **106**, 054302(5).
- 39 S. H. Chang and A. Taflove, *Opt. Express*, 2004, **12**, 3827–3833.
- 40 Y. Huang and S. T. Ho, *Opt. Express*, 2006, **14**, 3569–3587.
- 41 Y. Fu, H. Ågren, J. M. Kowalewski, H. Brismar, J. Wu, Y. Yue, N. Dai and L. Thylén, *Europhys. Lett.*, 2009, **86**, 37003(6).
- 42 H. Xu, L. Li, O. Manneberg, A. Russom, K. B. Gylfason, H. Brismar and Y. Fu, *J. Phys. Chem. B*, 2013, **117**, 14151–14156.
- 43 L. D. Landau and E. M. Lifshitz, *Quantum Mechanics*, Pergamon Press, Oxford, 2nd edn, 1965.
- 44 D. C. Reynolds, C. W. Litton and T. C. Collins, *Phys. Rev. B: Condens. Matter Mater. Phys.*, 1971, **4**, 1868–1872.
- 45 A. L. Pan, R. B. Liu and B. S. Zou, *Appl. Phys. Lett.*, 2006, **88**, 173102(3).
- 46 J. Urayama, T. B. Norris, J. Singh and P. Bhattacharya, *Phys. Rev. Lett.*, 2001, **86**, 4930(4).
- 47 Y. Fu, Y. H. Zhou, H. Su, F. Y. C. Boey and H. Ågren, *J. Phys. Chem. C*, 2010, **114**, 3743–3747.
- 48 Z. H. Chen, S. Hellström, Z. J. Ning, Z. Y. Yu and Y. Fu, *J. Phys. Chem. C*, 2011, **115**, 5286–5293.
- 49 C. de Mello Donegá, M. Bode and A. Meijerink, *Phys. Rev. B: Condens. Matter Mater. Phys.*, 2006, **74**, 085320(9).
- 50 M. Califano, A. Franceschetti and A. Zunger, *Phys. Rev. B: Condens. Matter Mater. Phys.*, 2007, **75**, 115401(7).
- 51 A. L. Efros, V. A. Kharchenko and M. Rosen, *Solid State Commun.*, 1995, **93**, 281–284.
- 52 V. I. Klimov and D. W. McBranch, *Phys. Rev. B: Condens. Matter Mater. Phys.*, 1999, **60**, 13740–13749.
- 53 K. Mukai, N. Ohtsuka, H. Shoji and M. Sugawara, *Appl. Phys. Lett.*, 1996, **68**, 3013–3015.
- 54 A. J. Nozik, *Annu. Rev. Phys. Chem.*, 2001, **52**, 193–231.
- 55 A. Pandey and P. Guyot-Sionnest, *Science*, 2008, **322**, 929–932.
- 56 T. Inoshita and H. Sakakia, *Physica B*, 1996, **227**, 373–377.
- 57 P. Frantsuzov, M. Kuno, B. Janko and R. A. Marcus, *Nat. Phys.*, 2008, **4**, 519–522.

